APENDIX-1
LIST OF PUBLICATIONS

[1]. M. Jagadeesh, **M. Lavanya**, S. K. Kalangi, Y. Sarala, C. Ramachandraiah, A. Varada Reddy, *"Spectroscopic characterization, antioxidant and antitumour studies of novel bromo substituted thiosemicarbazone and its copper(II), nickel(II) and palladium(II) complexes"* **Spectrochimica Acta Part A: Molecular and Biomolecular Spectroscopy** ***135 (2015) 180-184.***

[2]. M. Jagadeesh, **M. Lavanya**, B. Hari Babu, Kiryong Hong, Rory Ma, Joonghan Kim, Tae Kyu Kim, *"Synthesis and detailed spectroscopic characterization of various hydroxy-functionalized fluorescent chalcones: A combined experimental and theoretical study"* **Spectrochimica Acta Part A: Molecular and Biomolecular Spectroscopy** ***150 (2015) 557-564.***

Spectrochimica Acta Part A: Molecular and Biomolecular Spectroscopy 135 (2015) 180–184

Contents lists available at ScienceDirect

Spectrochimica Acta Part A: Molecular and Biomolecular Spectroscopy

journal homepage: www.elsevier.com/locate/saa

Spectroscopic characterization, antioxidant and antitumour studies of novel bromo substituted thiosemicarbazone and its copper(II), nickel(II) and palladium(II) complexes

M. Jagadeesh [a], M. Lavanya [a], Suresh K. Kalangi [b], Y. Sarala [c], C. Ramachandraiah [d], A. Varada Reddy [a,*]

[a] Department of Chemistry, Sri Venkateswara University, Tirupati, AP 517502, India
[b] School of Life Sciences, University of Hyderabad, Hyderabad, AP 500046, India
[c] Chemical Engineering Department, CBIT, JNTU, Hyderabad, 500072, India
[d] Department of Chemistry, Srikalahasteeswara Institute of Technology (SKIT), Srikalahasti, AP 517640, India

HIGHLIGHTS

- Copper(II), nickel(II) and palladium(II) complexes of DBAPTSC are synthesized.
- Tetragonally distorted octahedron copper(II) DBAPTSC is synthesized.
- Nickel(II) complex has shown good antitumour activity against HepG2 hepatoblastoma cell lines.
- The compounds are identified as semiconducting materials with the band gap data obtained from UV–visible spectra.

GRAPHICAL ABSTRACT

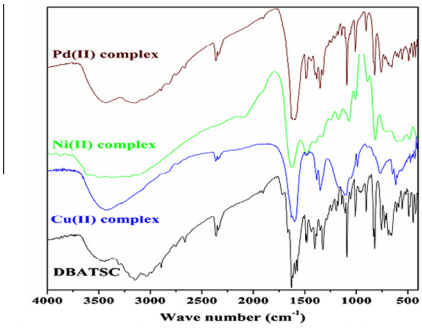

FT-IR spectra of DBATSC and its Cu(II), Ni(II) and Pd(II) complexes

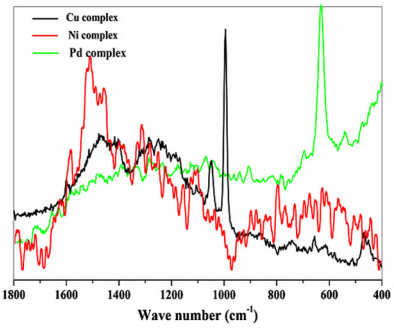

FT-Raman spectra of DBATSC and its Cu(II), Ni(II) and Pd(II) complexes

ARTICLE INFO

Article history:
Received 21 April 2014
Received in revised form 16 June 2014
Accepted 29 June 2014
Available online 8 July 2014

Keywords:
Dibromoacetophenone thiosemicarbazone
Transition metal complexes
EPR spectra
Antitumour activity

ABSTRACT

A new, slightly distorted octahedral complex of copper(II), square planar complexes of nickel(II) and palladium(II) with 2,4′-dibromoacetophenone thiosemicarbazone (DBAPTSC) are synthesized. The ligand and the complexes are characterized by FT-IR, FT-Raman, powder X-ray diffraction studies. The IR and Raman data are correlated for the presence of the functional groups which specifically helped in the confirmation of the compounds. In addition, the free ligand is unambiguously characterized by ^{1}H and ^{13}C NMR spectroscopy while the copper(II) complex is characterized by electron paramagnetic resonance spectroscopy (EPR). The g values for the same are found to be 2.246 (g_1), 2.012 (g_2) and 2.005 (g_3) which suggested rhombic distortions. The HOMO–LUMO band gap calculations for these compounds are found to be in between 0.5 and 4.0 eV and these compounds are identified as semiconducting materials. The synthesized ligand and its copper(II), nickel(II) and palladium(II) complexes are subjected to antitumour activity against the HepG2 human hepatoblastoma cell lines. Among all the compounds, nickel(II) complex is found to exert better antitumour activity with 57.6% of cytotoxicity.

© 2014 Elsevier B.V. All rights reserved.

Introduction

Thiosemicarbazones emerged as the versatile reagents that are playing prominent role in both qualitative analysis and quantitative [1,2] estimation of the trace metals and also in the bioinorganic field. Numerous thiosemicarbazone derivatives have been found to

* Corresponding author. Tel.: +91 9441408851; fax: +91 877 2246111.
E-mail address: ammireddyv@yahoo.co.in (A. Varada Reddy).

http://dx.doi.org/10.1016/j.saa.2014.06.141
1386-1425/© 2014 Elsevier B.V. All rights reserved.

possess good activity against human tumours [3]. Biological activities of these thiosemicarbazone moieties are found to have enormous increase after complexation with the transition metal ions [4,5]. They have been proved as the versatile agents exhibiting antimicrobial [6,7], antitumour [8], antifungal [9], antiviral [10] and enzyme inhibitors, etc. Use of copper(II) thiosemicarbazone complexes as radiopharmaceuticals is one of the most recent advances in the sulphur chemistry [11]. Coordination of the thiosemicarbazone ligand to metal ion has greatly increased the antimicrobial activity [12,13]. Differently substituted thiosemicarbazones on coordination to copper(II) and other transition metal ions have been identified as the compounds with high cytotoxicity towards the tumour cells in vivo and in vitro [14]. In the present study, the author concentrated more in the synthesis of the bromo-substituted thiosemicarbazone ligand and its respective copper(II), nickel(II) and palladium(II) complexes. The compounds are characterized by using different spectroscopic techniques. Antitumoral activity evaluation of the free ligand and the complexes against the human hepatoblastoma cell lines is also carried out.

Materials and methods

Chemicals

All the chemicals used in the present work are of analytical grade unless reported. The organic chemicals 2-bromo-1-(4-bromophenyl)ethanone is purchased from Avara synthesis Pvt. Ltd., thiosemicarbazide is obtained from Sd-Fine chemicals, $CuCl_2$ and other organic solvents are purchased from different commercial sources and are used without further purification.

Apparatus

A JASCO Corp., UV-530 spectrophotometer equipped with a 1.0 cm quartz cell is used for the absorbance studies. Infrared spectra are recorded as KBr pellets on JASCO FT-IR 4100 spectrophotometer (IIT MADRAS) in the range of 4000–400 cm^{-1}. The ^{1}H and ^{13}C NMR spectral analysis of the ligand DBAPTSC was done as DMSO-d^6 solutions by using tetramethylsilane (TMS) as the internal solvent on a Bruker-400 MHz instrument provided by the School of Chemistry, University of Hyderabad at 300 K. EPR spectra of the copper(II) complex is recorded as polycrystalline samples at 298 K on a Bruker-ER073 instrument equipped with an EMX microX source for X-band measurement using Xenon 1.1b.60 software provided by the manufacturer. Raman spectra are measured using a confocal Raman microscope (LabRam HR 800, Horiba JobinYvon SAS, France) equipped with a 432 nm He–Ne Laser (Torus Laser, Laser Quantum, France) with laser power 50 mW, 2 scans and a 50 X LWD air – dry visible objective (NA = 0.5 wd 10.6 MM LIEU Microsystems of Model BX 41) and attached with a Fieltiyar multichannel CCD detector. Each Raman spectrum is measured in the range of 400–1800 cm^{-1} with a spectral resolution of 0.35 cm^{-1}/pixel with 1800 gr/mm grating at the confocal pinhole is set to 400 nm. Lab Sepc software under windows is used to control the Raman system, form data acquisition and saving the data. X-ray powder diffraction data are collected on a Philips X'pert Pro X-ray powder diffractometer equipped with X'cellerator detector at room temperature. The scan range, step size, and time per step are 2θ = 5.00 to 40, 0.028 and 30 s, respectively.

Experimental

Synthesis of 2,4′-dibromoacetophenone thiosemicarbazone (DBAPTSC)

To a hot ethanolic solution of thiosemicarbazide (0.01 mol, 0.9102 g), solution of 2,4′-dibromoacetophenone (0.01 mol, 2.7794 g) is added slowly under constant stirring. A reddish brown coloured solution is formed after refluxion of the mixture for about 5 h. A yellowish brown coloured compound is obtained on evaporating the solvent under reduced pressure [15–17].

Synthesis of copper(II), nickel(II) and palladium(II) complexes

To 10.0 mL solution of the ligand in ethanol (0.002 mol, 0.6132 g), aqueous ethanolic solution of corresponding metal salt (0.001 mol) is added slowly under constant stirring in nitrogen atmosphere. The contents of the flask are then stirred at room temperature for 48 h to collect the dark coloured solution. The coloured solution is then allowed to evaporate at room temperature to obtain the coloured precipitate.

Antioxidant activity

To evaluate the radical scavenging activity of these compounds, a valid and standard method is employed using DPPH [18]. In DPPH method, the principle involved in evaluation of antioxidant activity is based on the conversion of DPPH into 1,1-diphenyl-2-picrylhydrazine. First preliminary analysis is carried out in order to check whether the compounds are active or not. A qualitative procedure is employed in which the sample compound (approximately 100 μg/mL) is applied as a spot on TLC plate and after the development of chromatogram using MeOH:CH_3CN (7:1) mobile phase, 0.2% DPPH (w/v) solution is sprayed on the plate. A yellow spot on the purple background indicates the antioxidant activity. For the quantitative estimation of scavenging activity, compounds are dissolved in 1% DMSO solution to give the 10.0 mL of stock solution (1.0 mg/mL). The stock is further diluted to get the sample solutions containing 25–100 μg/mL. To each sample solution containing the concentrations of 25–100 μg/mL, 3.0 mL of 0.004% methanolic DPPH (w/v) is added. After 30 min of incubation, the colour change is measured by taking the absorbance value at 517 nm using a Schimadzu UV–vis-2450 instrument. The absorbance values are compared with BHT (standard) concentrations of 25–100 μg/mL.

Antitumour activity

Cell viability is assessed by the MTT staining method [19]. Cells are harvested from 4 to 5-day-old cultures and are seeded in 96-well plates at the density of 5×10^3 cells. The HepG2 cells are treated with synthesized compounds with increasing concentrations of 20, 40, 60, 80 and 100 μM for 48 h in a final volume of 100 μL. At the end of the treatment, 20 μL of MTT (5 mg MTT/mL in PBS) is added and the cells are incubated for a further period of 4 h. In control experiments, cells are grown in the same media without the compounds. About 100 μL of DMSO is added to each culture and mixed by repeated pipetting and adding to dissolve the reduced MTT crystals. Relative cell viability is evaluated by measuring the optical density at 570 nm on microplate reader (Quant Bio-tek Instruments, Inc.). At 100 μM concentration of the synthesized compounds, three different experiments are carried out in triplicates and the mean values are reported as the cell cytotoxicity for each compound.

Result and discussion

^{1}H and ^{13}C NMR spectra of the ligand DBAPTSC

The NMR spectrum of the free ligand has provided significant evidence for the confirmation of the structure. The —NH_2 protons are observed as singlet at δ9.42 while, the —NH proton is seen as

a broad peak at δ10.21 ppm. The compound is found to be with the ***E***-confirmation which is proved from the appearance of the —NH_2 protons in between δ9–12 ppm due to the weak hydrogen bonding with the hydrazine nitrogen [20,21]. The methylenic protons are observed at δ4.01 ppm. Aromatic protons of the free ligand are observed in the range of δ7.2–7.6 ppm. Fig. S1 (supplementary material) shows the ^{1}H and ^{13}C NMR spectra of the ligand DBAPTSC.

Infrared and Raman spectra

Infrared spectroscopy, though a simple technique, provides important information in the preliminary conformation of the structural aspects of new molecules in the absence of the crystallographic data. The bands originating from the infrared spectra of the synthesized compounds revealed some interesting facts about the coordination behaviour of these NS donor ligands. In the IR spectrum of the ligand, showed sharp and intense band at 1629 cm^{-1}, a weak band at 1383 and a band at 833 cm^{-1} with a small shoulder among which the former one is assigned for the stretching mode of C═N bond of the ligand while the remaining bands are attributed for the stretching vibrations of the C═S bond. When turned to the IR spectrum of the complex the same bands corresponding for the stretching frequencies of the azomethine and thionic sulphur groups are observed at 1589(C═N) and 1349 and 761 cm^{-1}(C═S) respectively. The negative shift observed in the frequency of the azomethine and thione functions is attributed for the involvement of these groups in coordination with the copper(II) center [22]. Further the observance of the weak band at 449 cm^{-1} in the spectrum of the complex strongly suggests the formation of the Cu-N bond. In the case of free ligand a band at 3441(broad) and 3417 cm^{-1} indicates the presence of the NH_2 group. The bands are assigned for the asymmetric stretching vibrations of the NH_2 function coupled with the symmetric stretching vibration frequency. The square planar nickel(II) complex had represented similar behaviour in showing the stretching bands. The strong band at 1624 cm^{-1} which is slightly broad in nature is assumed to be because of the overlap of amine stretching band with the imine function. The thione function of the ligand after coordination has experienced relative decrease in bond order due to strong coordination with the metal ion which is seen at 816 cm^{-1} with a negative shift of 9 cm^{-1} (827 cm^{-1} for DBAPTSC). Finally, palladium(II) ion also involved in the formation of square planar complex with the strong and intense bands at 1589 and 822 cm^{-1} which are assigned for the coordinated imine and the thione functions of the ligand respectively. Fig. 1 shows the FT-IR bands for the free ligand DBAPTSC and its copper(II), nickel(II) and palladium(II) complexes.

Raman spectrum of the synthesized copper(II) complex had even supported the data obtained from the FT-IR spectrum by showing the characteristic bands at 1599 cm^{-1} (C═N) for azomethine group and bands at 1322 and 837 cm^{-1} assignable for the thione functions. For the nickel(II) complex, the Raman spectral data has shown the imine stretching band at 1589 cm^{-1} while the thione stretching is observed at 835 cm^{-1}. In the palladium complex the same are observed at a stretching frequency of 1582(C═N) and 831 cm^{-1} (C═S). Fig. 2 shows the FT-Raman spectra of DBAPTSC and its complexes.

Electronic spectra

The electronic spectra of the free ligand and its copper(II) complex is studied using a JASCO UV–vis-530 instrument as DMSO solutions (1×10^{-4} M). The ligand has shown a band at 352 nm (28,409 cm^{-1}), assigned for the intra ligand charge transfer $\pi \rightarrow \pi^*$ transition which is thought to be responsible for the brownish yellow colour of DBAPTSC. The electronic spectrum of the hexa coordinated copper(II) under the asymmetrical electronic distribution will split the ^{2}D term to B_{1g}, A_{1g}, B_{2g} and E_g levels. The spectrum of the complex has shown three bands υ_1, υ_2 and υ_3 at 295 (33,898 cm^{-1}), 344 (29,069 cm^{-1}) and 459 nm (21,786 cm^{-1}) respectively. The strong band υ_1 is assigned for the $\pi \rightarrow \pi^*$ transition of the ligand molecule associated with the iminic nitrogen function. The blue shift of the charge transfer transition band in the case of the copper(II) complex is thought to be because of the coordination of the copper(II) ion with the iminic nitrogen atom. The broad nature of the band is further explained because of the combination of N → Cu, ligand to metal charge transfer band [23,24]. The weak band appearing at 459 nm is assigned for the d-d transition associated with the S → Cu charge transfer. The nickel(II) complex has shown characteristic bands for square planar geometry. A strong LMCT band associated with $\pi \rightarrow \pi^*$ transitions of the phenyl ring at 383 nm (26,709 cm^{-1}) and a shoulder like peak at 437 nm (22,883 cm^{-1}) for $n \rightarrow \pi^*$ transition from the imine function of the ligand. The usual transitions of the square planar nickel(II) complexes are overlapped by the S → Ni charge transfer band. The blue shift and the broad nature of the $\pi \rightarrow \pi^*$ transitions in the case of nickel(II) complexes are associated with the coordination of

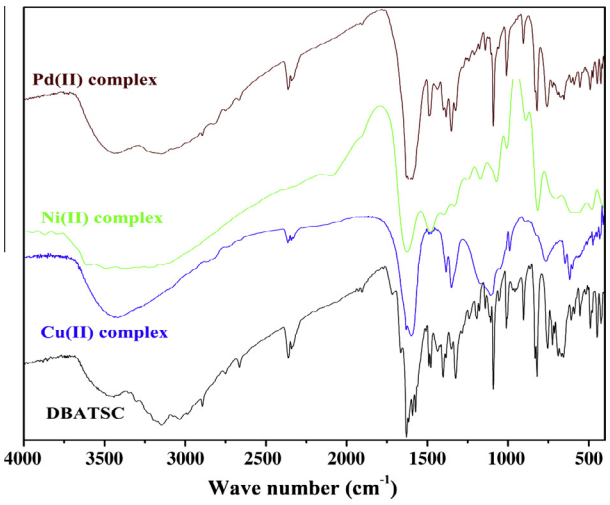

Fig. 1. Infrared spectra of DBAPTSC and its complexes recorded between 4000 and 400 cm^{-1}.

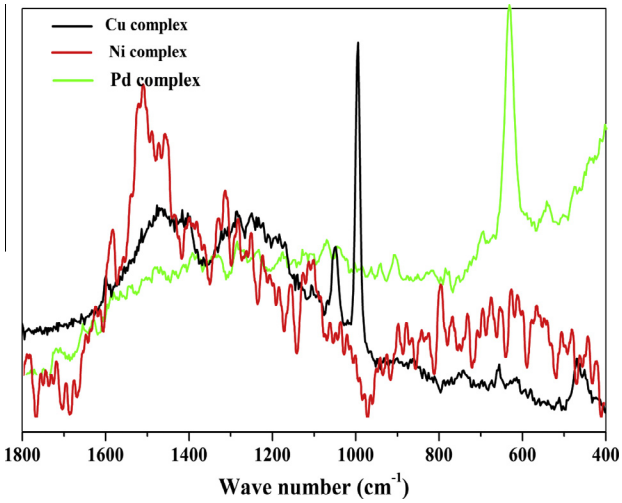

Fig. 2. FT-Raman spectra of the Cu(II), Ni(II) and Pd(II) complexes recorded from 1800 to 400 cm^{-1}.

the iminic nitrogen to the metal ion [25]. The band gap calculation from the UV–visible spectra is found to be 1.59 eV. Finally, the Palladium(II) complex has shown an electronic spectrum with three transitions $^1A_{1g} \rightarrow {}^1E_g$ (υ_1), $^1A_{1g} \rightarrow {}^1B_{1g}$ (υ_2) and $^1A_{1g} \rightarrow {}^1A_{2g}$ (υ_3) at 462 (43,668 cm^{-1}), 340 (29,411 cm^{-1}) and 301 nm (33,222 cm^{-1}) respectively. The band gap is found to be 2.10 eV imparting it the semiconducting property. Finally, the copper(II) complex is suggested to be paramagnetic while the nickel(II) and palladium(II) complexes are diamagnetic.

Electron paramagnetic spectra

The EPR spectrum of the copper(II) complex in polycrystalline state at 298 K has shown three bands with the g values, $g_1 = 2.246$, $g_2 = 2.012$ and $g_3 = 2.005$ suggesting the rhombic distortions. The EPR spectrum is found to be anisotropic since the g values are not equal to one other ($g_1 \neq g_2 \neq g_3$). Fig. 3 shows the EPR spectrum of the copper(II) complex derived from the ligand DBAPTSC.

Powder X-ray diffraction studies

Powder X-ray diffraction studies of the free ligand and its copper(II) complex suggested the high crystalline nature of these compounds at room temperature. Intense sharp peaks are observed in the spectrum of the copper(II) complex compared to the ligand indicating the increased crystalline nature after coordination with the copper(II) center while the nickel and palladium(II) complexes are semi crystalline in nature. The diffraction diagrams are shown in Fig. 4.

Antioxidant activity

The antioxidant activity of an inhibitor mainly depends on the way it participates in neutralizing the radical centers that are generated in the biological systems by donating an electron or hydrogen. The structure and properties of the inhibitor plays a prominent role in showing the activity. The newly synthesized ligand and its complexes are subjected to antioxidant activity assay using DPPH radical scavenging method [26]. A considerable increase in the percent of scavenging activity is found with increase in concentration of the compound except for Ni(II) complex. The free ligand DBAPTSC is found more efficient in decolorizing the pink colour of the DPPH solution than its copper(II) complex. While the palladium(II) complex of DBAPTSC has shown greater scavenging activity than copper(II) and nickel(II) complexes. The IC_{50} values are 0.76 mg/mL (DBAPTSC), 0.46 mg/mL (Cu(II) complex) and for 0.67 mg/mL (Pd(II) complex).

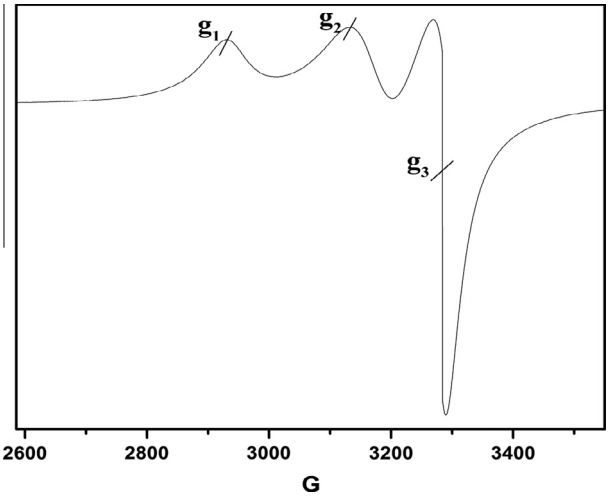

Fig. 3. EPR spectrum of the copper(II) complex.

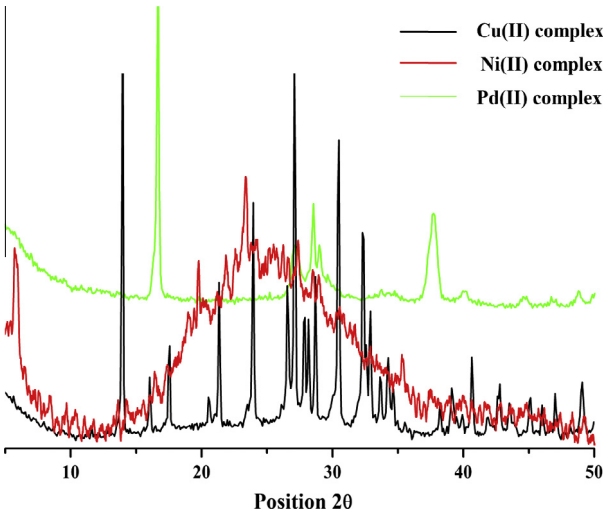

Fig. 4. Powder X-ray diffraction spectra of copper(II), nickel(II) and palladium(II) complexes at room temperature.

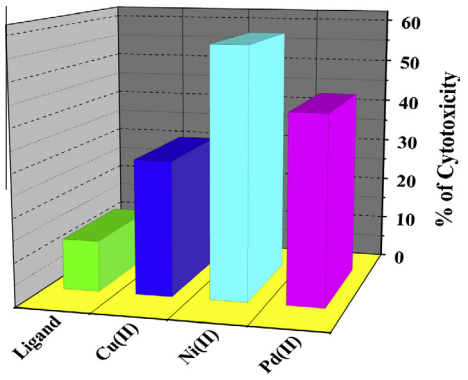

Fig. 5. Antitumour activity of the free ligand (DBAPTSC) and its copper(II), nickel(II) and palladium(II) complex against HepG2 human hepatoblastoma cell lines as % of cytotoxicity.

Antitumour activity

Results of the antitumour activity were evaluated by treating the compounds against the HepG2 human hepatoblastoma cell lines. The free ligand and its respective complexes have shown different order of activity. Fig. 5 shows the antitumour activity of the compounds in terms of percent of cytotoxicity activity. Among all the compounds, nickel(II) complex is found to be the most efficient one with 56.4% of cytotoxicity.

Conclusions

Finally, we conclude that, a novel bromo substituted thiosemicarbazone and its copper(II), nickel(II) and palladium(II) complexes are synthesized and finely characterized by using the different spectroscopic techniques. The coordination of the ligand to the metal ion is established with the help of the FT-IR and FT-Raman studies. The copper(II) complex has shown a tetragonally distorted octahedral geometry whose characteristic g values are calculated

from the EPR spectral information. Nickel(II) complex is the most effective antitumour agent when compared to palladium(II) and copper(II) complexes.

Acknowledgements

The author M. Jagadeesh extends his thanks to UGC-BSR for providing financial support in the form of RFSMS. The author also extends his heartfelt thanks to Prof. Samar K. Das, School of Chemistry and Prof. P. Reddanna, School of life Sciences, University of Hyderabad, Hyderabad for his help in providing the antitumoural studies in his laboratory.

Appendix A. Supplementary material

Supplementary data associated with this article can be found, in the online version, at http://dx.doi.org/10.1016/j.saa.2014.06.141.

References

[1] S. Lakshmi Narayana, K. Janardhan Reddy, S. Adi Narayana Reddy, Y. Sarala, A. Varada Reddy, Environ. Monit. Assess. 144 (2008) 341–349.
[2] K. Janardhan Reddy, J. Rajesh Kumar, C. Ramachandraiah, T. Triveni, A. Varada Reddy, Food Chem. 101 (2007) 585–591.
[3] A. Sertorelli, K.C. Agrawal, ACS Symp. Set. (1976) 301.
[4] X. Dong, Y. Li, Z. Li, Y. Cui, H. Zhu, J. Inorg. Biochem. 108 (2012) 22–29.
[5] D.V. Demertzi, A. Papageorgiou, L. Papathanasis, A. Alexandratos, P. Dalezis, J.R. Miller, M.A. Demertzis, Eur. J. Med. Chem. 44 (2009) 1296–1302.
[6] S. Chandra, S. Raizada, M. Tyagi, A. Gautam, Bioinorg. Chem. Appl. 2007 (2007) 1–7.
[7] M.C. Rodriguez-Arguelles, S. Mosquera-Vazquez, P. Touron-Touceda, J. Sanmartin-Matalobos, A.M. Garcia-Deibe, M. Belicchi-Ferrari, G. Pelosi, C. Pelizzi, F. Zani, J. Inorg. Biochem. 101 (2007) 138–147.
[8] F.A. Beckford, J. Thessing, A. Stott, A.A. Holder, O.G. Poluektov, L. Li, N.P. Seeram, Inorg. Chem. Comm. 15 (2012) 225–229.
[9] M.C. Rodriguez-Arguelles, P. Touron-Touceda, R. Cao, A.M. Garcia-Deibe, P. Pelagatti, C. Pelizzi, F. Zani, J. Inorg. Biochem. 103 (2009) 35–42.
[10] G. Pelosi, F. Bisceglie, F. Bignami, P. Ronzi, P. Schiavone, M. Carla Re, C. Casoli, E. Pilotti, J. Med. Chem. 53 (2010) 8765–8769.
[11] B.M. Paterson, P.S. Donnelly, Chem. Soc. Rev. 40 (2011) 3005–3018.
[12] R.A. Sanchez-Delgado, K. Lazardi, L. Rincon, J.A. Urbina, J. Med. Chem. 36 (1993) 2041–2043.
[13] I.C. Mendes, J.P. Moreira, A.S. Mangrich, S.P. Balena, B.L. Rodrigues, H. Beraldo, Polyhedron 26 (2007) 3263–3270.
[14] A.I. Matesanz, P. Souza, J. Inorg. Biochem. 101 (2007) 1354–1361.
[15] E. Franco, E. Lopez-Torres, M.A. Mendiola, M.T. Sevilla, Polyhedron 19 (2000) 441–451.
[16] M. Jagadeesh, H.K. Rashmi, Y. SubbaRao, A. Sreenath Reddy, B. Prathima, P. Uma Maheswari Devi, A. Varada Reddy, Spectrochim. Acta Part A Mol. Biomol. Spectrosc. 115 (2013) 583–587.
[17] M. Jagadeesh, Suresh K. Kalangi, L. Sivarama Krishna, A. Varada Reddy, Spectrochim. Acta Part A Mol. Biomol. Spectrosc. 118 (2014) 552–556.
[18] A. Braca, N.D. Tommasi, L.D. Bari, C. Pizza, M. Politi, I. Morelli, J. Nat. Prod. 64 (2001) 892–895.
[19] T. Mosmann, J. Immunol. Methods 65 (1983) 55.
[20] A.A. Ali, H. Nimir, C. Aktas, V. Huch, U. Rauch, K-H. Schafer, M. Veith, Organometallics 31 (2012) 2256.
[21] M. Jagadeesh, V. Asha Kumar, C. Ramachandraiah, A. Varada Reddy, J. Appl. Pharm. Sci. 3 (7) (2013).
[22] P.F. Rapheal, E. Manoj, M.R. Prathapachandra Kurup, Polyhedron 26 (2007) 818–828.
[23] Ana I. Matesanz, J. Perles, P. Souza, Dalton Trans. 41 (2012) 12538–12547.
[24] U.L. Kala, S. Suma, M.R. Prathapachandra Kurup, Suja Krishnan, Rohit P. John, Polyhedron 26 (2007) 1427–1435.
[25] L. Sacconi, M. Ciampolini, G.P. Speoni, J. Am. Chem. Soc. 87 (1965) 3102–3106.
[26] R.N. Patel, N. Singh, K.K. Shukla, V.L.N. Gundla, Spectrochim. Acta Part A Mol. Biomol. Spectrosc. 61 (2005) 1893–1897.

Spectrochimica Acta Part A: Molecular and Biomolecular Spectroscopy 150 (2015) 557–564

Contents lists available at ScienceDirect

Spectrochimica Acta Part A: Molecular and Biomolecular Spectroscopy

journal homepage: www.elsevier.com/locate/saa

Synthesis and detailed spectroscopic characterization of various hydroxy-functionalized fluorescent chalcones: A combined experimental and theoretical study

M. Jagadeesh [a], M. Lavanya [b], B. Hari Babu [c], Kiryong Hong [a], Rory Ma [a], Joonghan Kim [d,*], Tae Kyu Kim [a,*]

[a] Department of Chemistry and Chemical Institute of Functional Materials, Pusan National University, Busan 609-735, Republic of Korea
[b] Department of Chemistry, Sri Venkateswara University, Tirupati 517502, Andhra Pradesh, India
[c] Department of Surgery, Montreal General Hospital, McGill University, Montreal, Canada
[d] Department of Chemistry, The Catholic University of Korea, Bucheon 420-743, Republic of Korea

HIGHLIGHTS

- Interpretations of IR and Raman spectra of hydroxyl-substituted chalcones.
- Prepared hydroxyl-substituted chalcones as good semiconducting materials.
- The white-light emitting property of prepared hydroxyl-substituted chalcones.

GRAPHICAL ABSTRACT

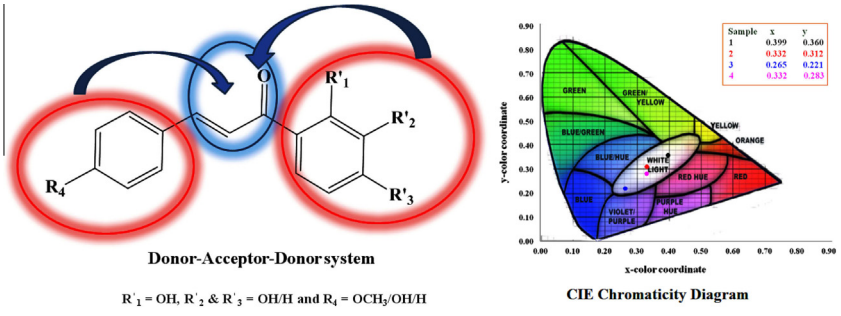

ARTICLE INFO

Article history:
Received 2 January 2015
Received in revised form 16 May 2015
Accepted 20 May 2015
Available online 9 June 2015

Keywords:
Hydroxy-substituted chalcones
DFT calculations
HOMO–LUMO
Vibrational spectra

ABSTRACT

Four different bright yellow to orange hydroxy-substituted chalcones (i.e., 2′,4-di-hydroxy (**1**), 2′,3′,4-trihydroxy (**2**), 2′,3′,4′-trihydroxy (**3**), and 2′-hydroxy-4-methoxy (**4**) chalcones) were synthesized and characterized by LC–MS, FT-IR, FT-Raman, and fluorescence spectroscopy and thermogravimetric analysis. UV–visible absorption spectroscopy was also used. The experimental (theoretical) bandgaps of **1**, **2**, **3**, and **4** are 2.89 (2.90), 2.93 (2.95), 3.04 (3.09), and 3.01 (2.91) eV, respectively. The hydroxy-substituted chalcones exhibited strong dual emissions as a consequence of the locally excited states followed by internal charge transfer processes. The molecular structures, lowest energy transitions, vibrational frequencies, and spectroscopic information were calculated using density functional theory and time-dependent density functional theory methods at the B3LYP/6-31G(d,p) theoretical level. The experimental and theoretical data were compared and the relationship between them was briefly discussed.

© 2015 Elsevier B.V. All rights reserved.

Introduction

Benzylideneacetophenones, which are commonly known as chalcones, have gained significant attention in modern chemistry because of their wide range of applications [1]. These bichromophoric molecules, which have two chromophoric groups separated by a hetero-vinyl chain, serve as precursors of several heterolytic compounds like flavonoids, flavones, and pyrazolones [2–5]. Chalcones are excellent models for studying photo-induced electron transfer processes, which play a key role in different fields such as polymer, photo, optic, and laser physics [6,7]. These chromophores, which feature electron-donor and

* Corresponding authors.
E-mail addresses: joonghankim@catholic.ac.kr (J. Kim), tkkim@pusan.ac.kr (T.K. Kim).

http://dx.doi.org/10.1016/j.saa.2015.05.085
1386-1425/© 2015 Elsevier B.V. All rights reserved.

electron-acceptor groups connected via a π-conjugated spacer, are called donor–π–acceptor (D–π–A) systems [8]. Chalcones are classified into symmetrical and asymmetrical donor–acceptor–donor (D–A–D) systems based on the electron-donating substituents attached to the aromatic rings at the end of the carbonyl functional group: Symmetrical D–A–D chalcones contain electron donors on both phenyl rings, while asymmetrical D–A–D chalcones have electron donors at only one of the two phenyl rings [9]. Hence, these molecules can show highly efficient intramolecular charge transfers, and thus they are particularly useful in the development of nonlinear optical systems (NLO materials) [10]. They are also used for ultrafast optical nonlinearities [11] and as absorption filters for UV light [12].

Among the various chalcone derivatives, hydroxy chalcones and related derivatives have proven to be challenging candidates that attract wide biological interest. For example, a number of pharmacological applications of these derivatives have been investigated because of their antitumor [13–15], antidiabetic [16], antimalarial [17], antioxidant [18], antifungal [19], anti-angiogenic [20], and anti-inflammatory activities [21]. In particular, electron-releasing groups that induce high polarization of the ring enhance the antibacterial [22–24] and enzyme-inhibition activity [25,26]. In addition, 2′-hydroxy chalcones like chalcone **1** and **4** are suitable for quantitative analysis of metal ions because of their good complexing ability [27]. The applications of chalcones also extend to agrochemicals and artificial sweeteners [7].

Although hydroxy-substituted chalcones have a variety of applications, especially in pharmacological fields, detailed elucidations of the structural and spectroscopic properties of these hydroxy-substituted chalcones have rarely been reported. Detailed spectroscopic assessments may aid in generating facile syntheses of new chalcone derivatives and advance the pharmacological applications of hydroxy-substituted chalcones. In this work, we report the preparation and structural elucidation of four hydroxy-substituted chalcones, i.e., 2′,4-dihydroxychalcone (**1**), 2′,3′,4-trihydroxychalcone (**2**), 2′,3′,4′-trihydroxychalcone (**3**), and 2′-hydroxy-4-methoxychalcone (**4**) using a variety of spectroscopic methods. In addition, theoretical approaches including DFT and TD-DFT calculations are used to study their molecular vibrations, frontier orbitals, and electronic transitions. The experimental and calculation data are compared and the relationship between them is briefly discussed.

Materials and methods

Chemicals and syntheses of hydroxy chalcone derivatives

All chemicals and solvents used in the present work were obtained from commercial sources and used without any further purification. 4-Hydroxybenzaldehyde, 2′-hydroxyacetophenone, 2′,4′-dihydroxyacetophenone, benzaldehyde, 2′,3′,4′-trihydroxyacet o-phenone, and 4-methoxybenzaldehyde were purchased from Sigma Aldrich. The target chalcones were prepared according to the conventional base-catalyzed Claisen–Schmidt reaction as per the literature [28]. Equivalent molar amounts of an ethanolic solution of the hydroxy-substituted acetophenone with the corresponding benzaldehyde were mixed in a round-bottom flask. After adding 10% NaOH solution, the mixture was stirred at room temperature for 8–10 h. After complete consumption of the corresponding aldehyde, the solution was neutralized using 10% HCl. The precipitate was collected by filtration, dried, and recrystallized from ethanol.

Spectroscopic characterizations

FT-IR spectral measurements were recorded in the solid state using KBr pellets on a JASCO FTIR 5300 spectrophotometer between 4000 and 400 cm^{-1}. UV–visible spectra of the synthesized compounds were recorded using a JASCO V-570 UV–visible spectrophotometer. Mass spectra of the molecules were recorded using an Agilent Technologies 6530 Accurate Mass Q-TOF LC/MS. Raman spectra were measured using a confocal Raman microscope (Lab Ram HR 800, Horiba Jobin Yvon SAS, France) equipped with a 432 nm He-Ne laser (Torus Laser, Laser Quantum, France) at a power of 50 mW and a 50× LWD air-dry visible objective (NA = 0.5 wd 10.6 MM LIEU Microsystems of Model BX 41) that was attached to a Fieltiyar multichannel CCD detector; two scans were recorded. Each Raman spectrum was measured in the range of 400–1800 cm^{-1} at a spectral resolution of 0.35 cm^{-1}/pixel with an 1800 g/mm grating at the confocal pinhole, which was set at 400 nm. Fluorescence studies of the solid samples were recorded using a Hitachi F-7000 fluorescence spectrophotometer at room temperature. The chalcones were thermally analyzed using a Labsys TG-DSC 1600 model instrument under a N_2 atmosphere at a scan rate of 10 °C/min. Scanning electron microscopy (SEM) images of the chalcone molecules were obtained using a Carl Zeiss EVO MA 15 Thermonic Emission scanning electron microscope.

DFT calculations

To determine the properties of these chalcone molecules (**1–4**) at the molecular level, density functional theory (DFT) [29,30] was employed. The geometries of the chalcone molecules were fully optimized using Becke's three parameter hybrid functional [31] combined with the Lee, Yang, and Parr [32] correlation functional (B3LYP) using the standard Pople basis set, i.e., 6-31G(d,p), [33,34] for all atoms (i.e., H, C, N, and O atoms) in the gas phase. To validate that these optimized structures were global minima, the vibrational frequencies were also calculated using the same level of theory. Moreover, time-dependent DFT (TDDFT) calculations were used to investigate the optical properties of these four chalcone molecules. The DFT-optimized structures were employed and the same level of theory was used for TDDFT. We also used an integral equation formalism variant of the polarizable continuum model (IEFPCM) [35,36] for ethanol to account for the bulk solvent effects for all TDDFT calculations. All DFT and TDDFT calculations were performed using the Gaussian 09 program [37].

Results and discussion

FT-IR and FT-Raman spectral investigations

FT-IR spectroscopy can serve as an important basic tool for characterization of organic and inorganic molecules. In this work, experimental IR spectra of hydroxy chalcones (**1–4**) were compared and analyzed with respect to those obtained from DFT calculations (B3LYP/6-31G(d,p) level). The DFT-optimized molecular structures of **1–4** are shown in Fig. 1. The FT-IR and FT-Raman spectra of the synthesized chalcone derivatives are shown in Figs. 2 and 3, respectively. The theoretical spectra are also shown for comparison. We assigned only the important peaks in the FT-IR and FT-Raman spectra because there are only a limited number of references for the IR spectra of other chalcone molecules for comparison. As shown in Figs. 2 and 3, the experimental patterns of the IR and Raman peaks are much more complex because of overlapping peaks and the presence of highly active vibrational groups. The specified vibrations that occur at similar

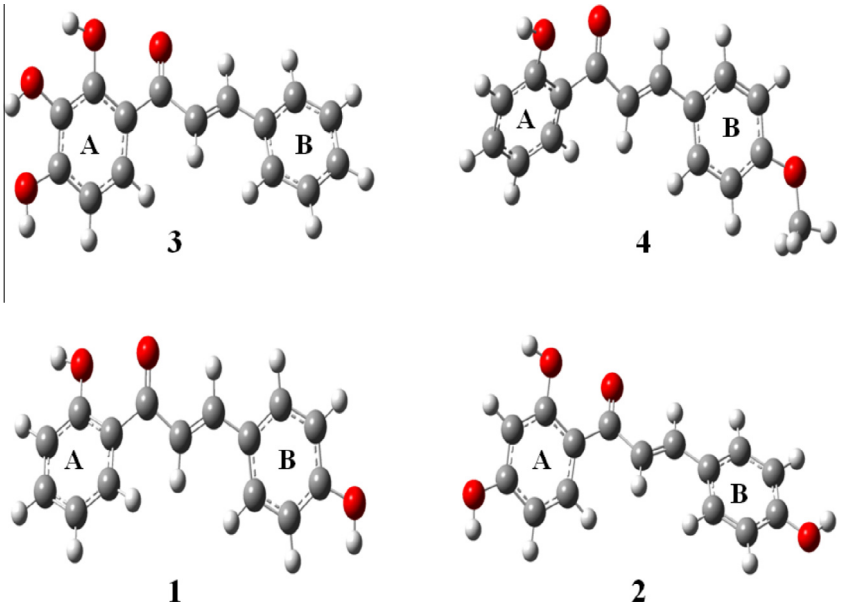

Fig. 1. Optimized structures of chalcones **1–4** from DFT calculations performed at the B3LYP/6-31G(d,p) level.

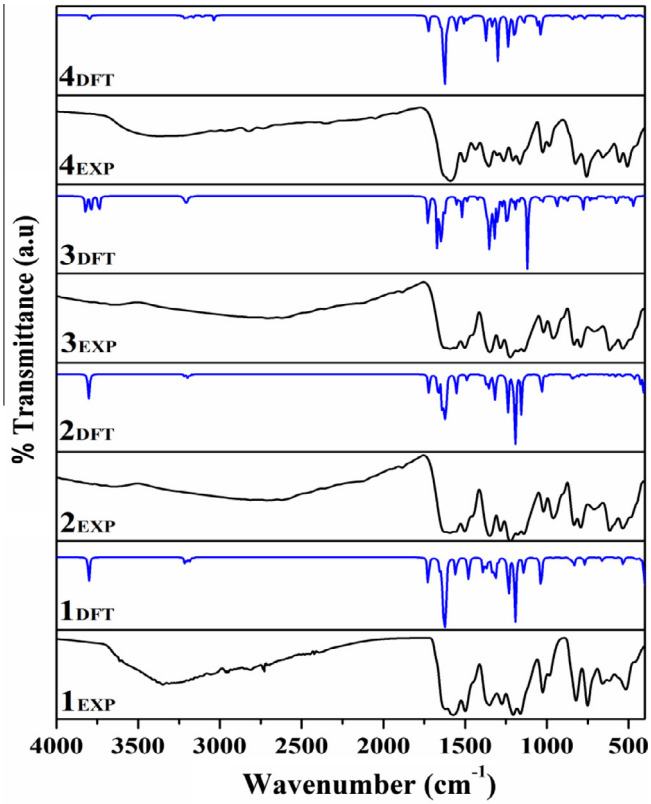

Fig. 2. FT-IR spectra of chalcones **1**, **2**, **3** and **4** recorded from 4000 to 400 cm^{-1}. The experimental spectra are shown in black and theoretical spectra are shown in blue. (For interpretation of the references to colour in this figure legend, the reader is referred to the web version of this article.)

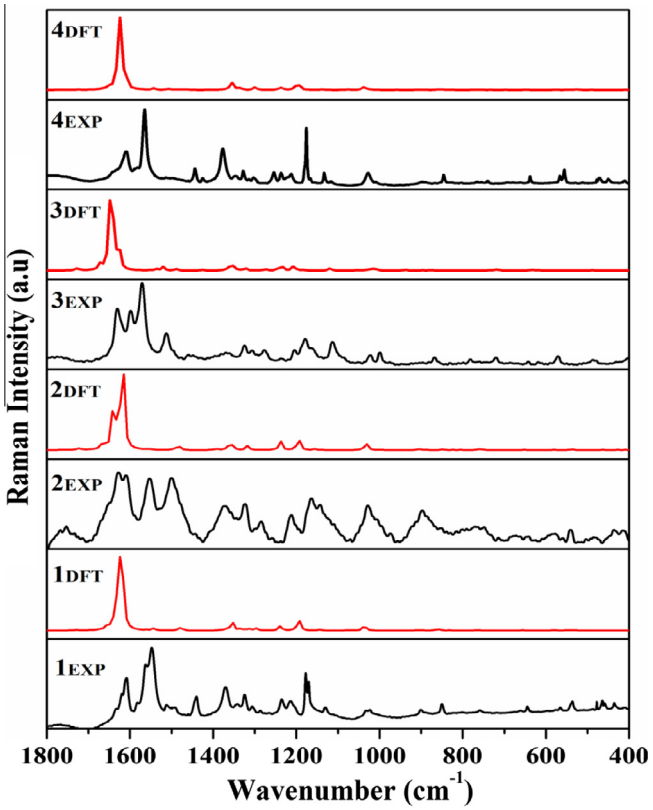

Fig. 3. FT-Raman spectra of the synthesized chalcones **1**, **2**, **3** and **4** recorded from 1800 to 400 cm^{-1}. The experimental spectra are shown in black and theoretical spectra are shown in red. (For interpretation of the references to colour in this figure legend, the reader is referred to the web version of this article.)

wavenumbers/range are assigned in details for each of the molecules (**1–4**). Tables S1–S4 in the Supplementary Material clearly show the overlapping bands occurring at specific wavenumbers; for instance, the hydrogen bonded carbonyl group overlapped by the aromatic C=C bond vibrations and the hydrogen bonded OH functional group overlaps with the aromatic C–H stretching vibrations. In the previous study [38], the intramolecular hydrogen bonding in 2′-hydroxy chalcones allows these molecules to exhibit *cis*-to-*trans* isomerization which further influences the spectroscopic properties. The theoretical spectra deviate from the experimental spectra, because the former was performed on a free molecule in vacuum ignoring the molecular interactions. While, the later was obtained for solid samples in which the molecules are strongly involved with interactions such as hydrogen bondings.

Moreover, the neglecting of anharmonicity might be a major cause for the deviation and complexity in the vibrational frequencies. The possibility of exhibiting conformational isomerism by these molecules can also be taken as one of the main causes for bringing complications in the experimental spectra [39–41].

C═O vibrations

Identification and assignment of the carbonyl group in the chalcones is crucial because of several factors, such as resonance, intra- and/or intermolecular hydrogen bonding, and type of substituent attached to the phenyl rings, affect the stretching vibrations of the α–β unsaturated carbonyl group. In chalcone **1**, the carbonyl group produced intense peaks at 1628 and 1634 cm^{-1} in the experimental IR and Raman spectra, respectively, and a sharp peak at 1725 cm^{-1} in the calculated IR spectra. In **2**, the corresponding peaks appeared at 1751 and 1793 cm^{-1} in the experimental spectra and 1721 cm^{-1} in the DFT-IR spectrum. The bands at 1632 (DFT: 1630) and 1725 (DFT: 1638) cm^{-1} of **3** in the IR and Raman spectrum, respectively, were attributed to the stretching vibrations of the carbonyl group. Chalcone **4** exhibits the same band structures at 1596 (DFT: 1608) and 1725 (DFT: 1622) cm^{-1} in the IR and Raman spectra, respectively. It is notable that the vibrational frequencies in both the IR and Raman experimental spectra are red-shifted relative to those in the DFT-calculated spectra of the optimized structures of the hydroxy chalcones; this indicates the strong involvement of the 2′-hydroxy functional group in intramolecular hydrogen bonding in the hydroxy chalcone derivatives. Several basic factors such as inductive and mesomeric effects will significantly shift the carbonyl stretching frequencies in carbonyl functional groups in aldehydes and ketones. The vibrational frequency of this group mainly depends on the force constant, which in turn is influenced on inductive, conjugative, field and steric effects. The presence of 4/4′-donor groups promotes the delocalization of π electrons via α–β unsaturation, which decreases the C═O bond order and thus increases the bond order between the carbonyl carbon and α carbon atom [40,41].

Aromatic C═C vibrations

In chalcone **1**, aromatic C═C bond stretching of the two phenyl rings is observed at 1606 cm^{-1} in the Raman spectrum and 1620 cm^{-1} in both the DFT-IR and DFT-Raman spectra. In the experimental IR spectrum, the corresponding peak overlaps with the carbonyl stretching band. For chalcone **2**, the band corresponding to the carbonyl group dominates the aromatic C═C stretching peak in the IR spectrum; the same peak appears with medium intensity in the Raman (1628 cm^{-1}), DFT-IR (1626 cm^{-1}), and DFT-Raman (1618 cm^{-1}) spectra. Compound **3** exhibits C═C vibrational bands in both the experimental and theoretical spectra. The corresponding bands are observed in the IR (Raman) experimental and DFT spectra at 1632 (1638) and 1630 (1638) cm^{-1}, respectively. In the case of **4**, the presence of the strong mesomeric group at the para position of the phenyl ring significantly influences the carbonyl functional group. As a result, no band is observed for the C═C bond vibration at the specified wavenumber that correlates with the band observed in the theoretical spectra. In the DFT-calculated IR and Raman spectra of chalcone **4**, the bands at 1622 cm^{-1} were assigned to the C═C vibrations.

O–H bond vibrations

As a result of the hydrogen bonding in the hydroxy-functionalized chalcones, significant deviation between the experimental and theoretical IR and Raman spectra is expected.

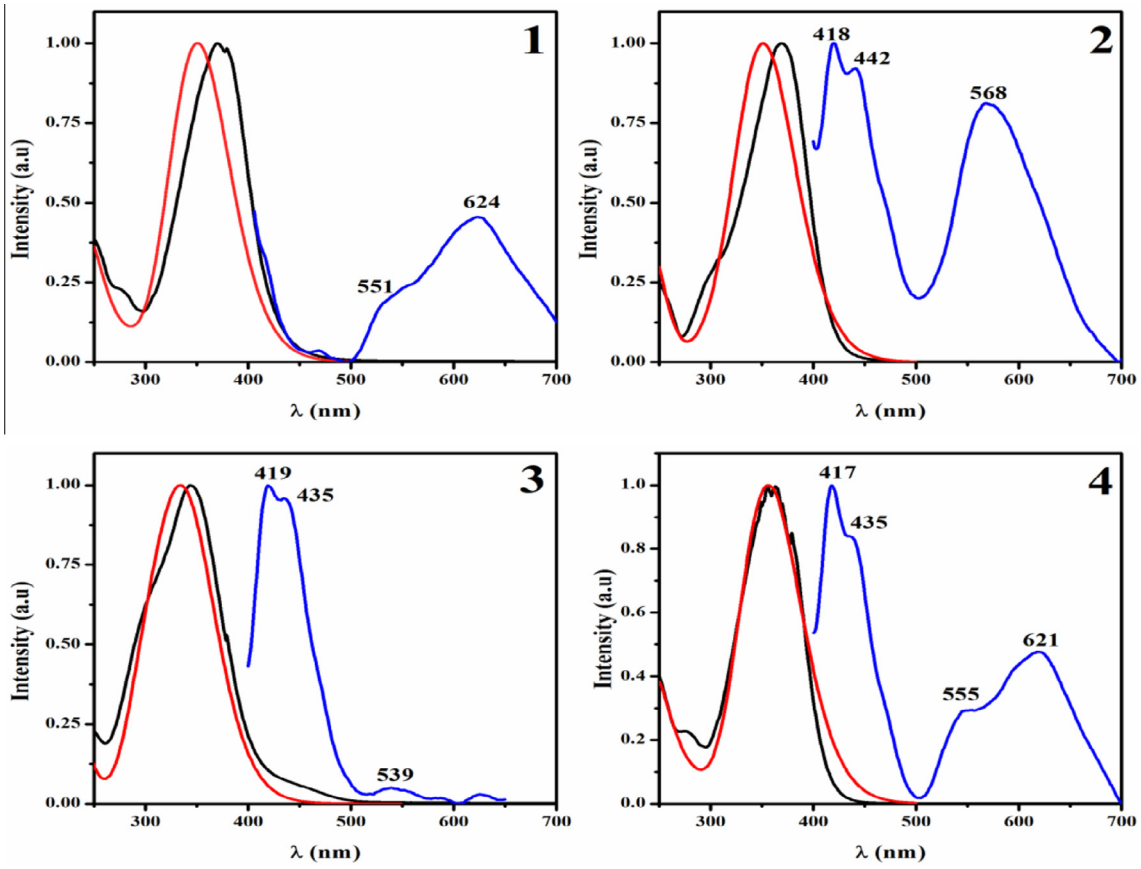

Fig. 4. Normalized absorbance spectra of **1**–**4** recorded in ethanol as a solvent: experimental (black), TD-DFT (red), and fluorescence (blue). (For interpretation of the references to colour in this figure legend, the reader is referred to the web version of this article.)

As shown in Figs. 2 and 3, the peaks for the O–H bond vibrations in the experimental IR and Raman spectra are at very different positions than those in the theoretical spectra. Broad and strong vibration peaks are evident at 3350, 3500, 3462, and 3442 cm^{-1} in the experimental FT-IR spectra of **1**, **2**, **3**, and **4**, respectively; these indicate the presence of the O–H bond, where the hydrogen atom is involved in hydrogen bonding with the carbonyl oxygen. The corresponding peaks in the DFT-IR spectra, in which intramolecular hydrogen bonding is ignored, are apparent at 3799, 3796, 3739, and 3797 cm^{-1} for **1**, **2**, **3**, and **4**, respectively.

C–H vibrations

The C–H bond vibrations can be categorized into two types based on the nature of the carbon atom: Aliphatic and aromatic. Chalcone **1** shows characteristic aromatic C–H vibrations at 3216 and 3215 cm^{-1} in the calculated IR and Raman spectra, respectively. Although most of corresponding peaks in the experimental IR and Raman spectra overlap with the O–H stretching band, several aromatic C–H vibrational peaks due to out-of-plane bending vibrations are evident at 821 and 847 cm^{-1} in the experimental IR and Raman spectra, respectively, and at 843 cm^{-1} in the DFT-IR spectrum. For **2**, the C–H vibration at 3218 cm^{-1} in the DFT-IR spectra is significant, but the corresponding peak in the experimental spectra is dominated by the O–H vibrational peak, as is the case for **1**. Out-of-plane bending modes in **2** are apparent at 875 and 894 cm^{-1} in the experimental data, while the same peaks are observed at 843 and 847 cm^{-1} in the DFT-calculated spectra. For **3** and **4**, the C–H vibrations effectively overlap with the O–H vibrations because of the increased number of hydroxy groups and resultant peak broadening. In the DFT-IR and DFT-Raman spectra, the C–H vibrational peaks are at 3205 and 3214 cm^{-1}, respectively. The additional peaks at 3164 and 3035 cm^{-1} in the IR and Raman spectra respectively of chalcone **4** were attributed to the asymmetric and symmetric stretching vibrations of the methoxy-methyl protons.

UV–visible absorption spectra

UV–visible spectra of the synthesized hydroxy chalcone derivatives in ethanol solution are shown in Fig. 4; theoretical UV–visible spectra obtained from TD-DFT calculations of the optimized ground state geometries of **1**–**4** are also shown for comparison. The synthesized chalcones contain a hydroxy-substituted aromatic carbonyl group with continuous conjugation that shows two predominant $n \rightarrow \pi^*$ and $\pi \rightarrow \pi^*$ electronic transitions in the UV–visible region. The two chromophoric groups at the ends of the carbonyl group in **1**–**4** produce the colors of the synthesized compounds, which range from bright yellow (**1**) to orange-red (**4**). The electron-donating hydroxy and methoxy groups are responsible for promotion of the donor character of the chromophores toward the carbonyl functional group, which acts as an acceptor. The absorption maxima of these compounds are evident in the near UV region, i.e., at 370 (350), 368 (351), 343 (334), and 363 (356) nm in the experimental (TD-DFT) absorption spectra of chalcones **1**, **2**, **3**, and **4**, respectively. The similarity of the absorption maxima of the experimental and TD-DFT results clearly confirms the accuracy of our theoretical method. The slight deviation of the TD-DFT spectra from the experimental spectra was attributed to the effects of inter- and intramolecular hydrogen bonding in **1**–**4**, which are not considered in the theoretical calculations. The small differences in the absorption spectra of **1**–**4** indicate that the distributions of the molecular orbitals (and their relative energies) are

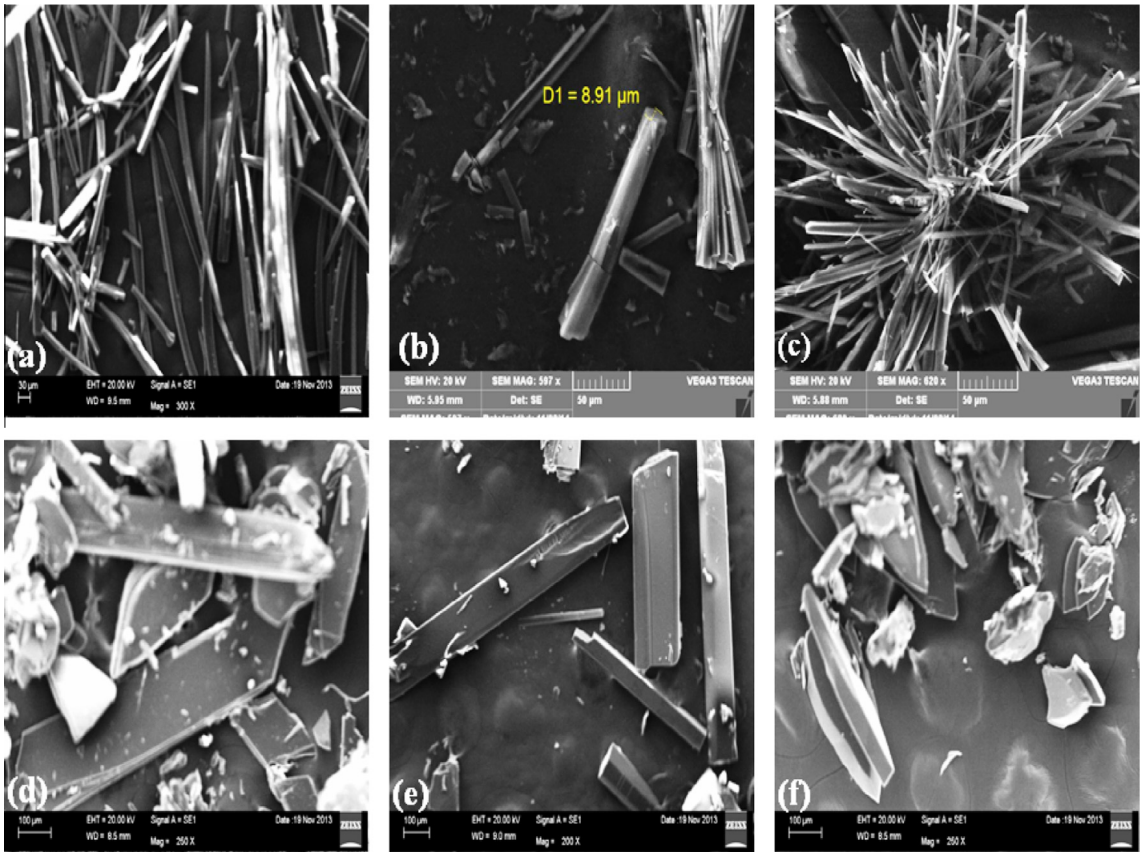

Fig. 5. SEM images of chalcones **1**–**4**: (a) chalcone **1**, (b and c) epitaxial growth of the crystals of chalcone **1** after recrystallization in ethanol, (d) chalcone **2**, (e) chalcone **3**, and (f) chalcone **4**.

similar. The energy difference between the ground and excited states, i.e., the bandgap or highest occupied molecular orbital (HOMO)–lowest unoccupied molecular orbital (LUMO) gap, was calculated from the UV–visible absorption spectra. To calculate the bandgap, the low-energy region of the spectrum (i.e., the absorption edge) was selected and an imaginary line that intersects the *x*-axis on an extrapolation of the linear part of the spectrum was substituted into the Planck equation, as follows:

$$E(\mathrm{J}) = \frac{hc}{\lambda\ (\mathrm{m})}. \quad (1)$$

Alternatively, the bandgap (in units of eV) can be obtained directly from

$$E\ (\mathrm{eV}) = \frac{1239.84187\ (\mathrm{eV\ nm})}{\lambda\ (\mathrm{nm})} \quad (2)$$

According to the bandgap calculations using Eq. (2), the four chalcones have bandgap energies between 0.5 and 4.0 eV and are therefore suitable as semiconductor materials. The experimental and calculated (given in brackets) bandgaps derived from the UV–visible spectra were 2.89 (2.90), 2.93 (2.95), 3.04 (3.09), and 3.01 (2.91) eV for compounds **1**, **2**, **3**, and **4**, respectively [42]. The low energies of these bandgaps were attributed to the presence of one or more positive mesomeric substituents (–OH and/or $-OCH_3$) on the phenyl rings; enhancement of the π-conjugation also decreased the bandgap between the HOMO and LUMO orbitals. It is noteworthy that the presence of one or more electron-donating functional groups in **1**–**4** facilitates the electron-transfer process to the carbonyl functional group; thus, these compounds can be considered as D–A–D-type molecules [43], as shown in the Supplementary data (Fig. S8). In general, the molecular arrangements in **1**–**4** strengthen the intramolecular charge transfers (ICTs).

HOMO–LUMO calculations

The frontier molecular orbitals, which comprise the HOMO and LUMO, play an important role in the optical and electrical properties and UV–visible spectra of molecules [44,45]. The optimized structures (Fig. 1) of chalcones **1**–**4** were used for visualization of the HOMO and LUMO orbitals using DFT. The distribution of the HOMO and LUMO orbitals were computed using the B3LYP/6-31G(d,p) method at the ground states of the optimized structures and are shown in Fig. S6 (Supplementary data). In chalcones **1** and **4**, the HOMO orbitals are primarily concentrated on ring B, which contains electron-releasing or positive mesomeric groups like –OH/$-OCH_3$ at the 4-position. In chalcone **2**, the HOMO orbital is evenly distributed between ring A and B because of the presence of donor groups on both rings. In contrast, chalcone **3** exhibits a different pattern with the HOMO orbitals located only on ring A because of the absence of such donor groups on ring B. The LUMO orbitals are primarily distributed on the acceptor part of the chalcone moieties, i.e., the carbonyl groups [43].

Fluorescence spectra

The normalized fluorescence emission spectra of chalcones **1**–**4** are shown in Fig. 4. All synthesized chalcone derivatives show

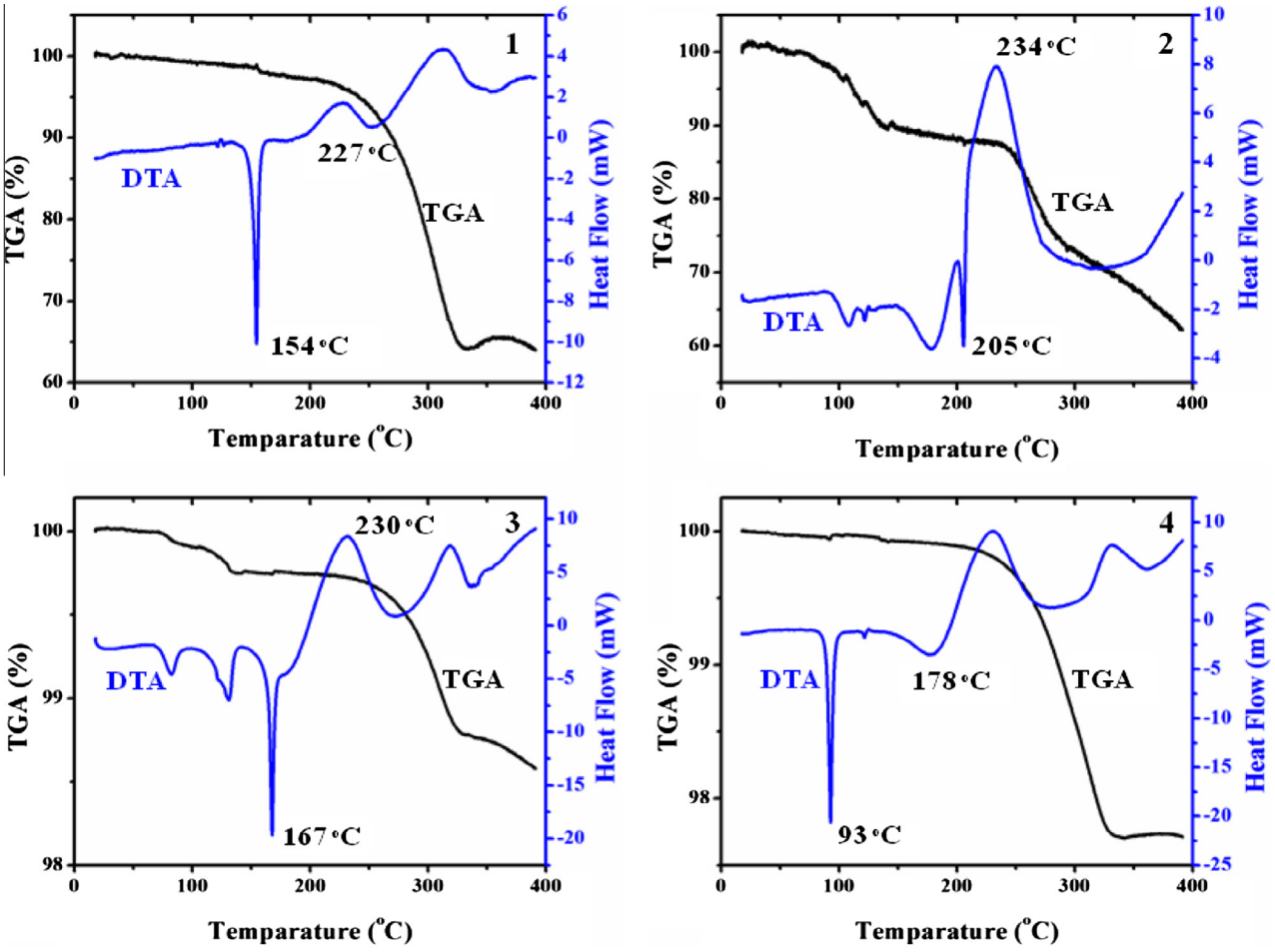

Fig. 6. Thermograms of chalcones **1**–**4** showing the response to increasing temperature from 20 to 400 °C in a N_2 atmosphere.

long-range emissions with corresponding emission maxima. Chalcone **1** exhibits a strong emission band from 700 to 500 nm, which covers the red to green region, with emission maxima at 624 and 551 nm. On the other hand, **2** and **4** show dual-emission with emission maxima at 418, 442, and 568 nm for **2** and 417, 435, 555, and 621 nm for **4**. In contrast, chalcone **3** only shows a high emission band at around 419 nm, which indicates suppression of the low-energy emission. The general dual-emission shapes of the spectra for **1**–**4** was attributed to the generation of a local excited state, which is followed by a photo-induced ICT [43]; however, the mechanism of this process is under debate [46]. The electron push–pull architecture of these molecules is responsible for the increased fluorescence. The emission colors of the chalcones were quantitatively characterized using the Commission Internationale de l'Éclairage (CIE) chromaticity coordinates. Fig. S7 (Supplementary data) shows the CIE chromatogram of the synthesized chalcone derivatives. From the CIE chromatogram, it is evident that the chalcones emit white light because of the additive mixing of the emitted color wavelengths; therefore, they are suitable for the development of organic light-emitting diodes (OLEDs).

Scanning electron microscopy

To evaluate the morphologies of the synthesized chalcones, we obtained SEM images of crystallized chalcone derivatives **1**–**4**, as shown in Fig. 5. Chalcone derivative **1** has a rod-like shape in the micrometer size range; however, upon treatment with ethanol, the crystals of chalcone **1** aggregate into a bushy structure because of epitaxial growth of the crystal from the center, as shown in Fig. 5(b) and (c). In contrast, chalcone derivatives **2**–**4** crystallize into sheets (layers) owing to the enhanced intermolecular interactions.

Thermogravimetric analysis

To assess the thermal stability of these fluorescent chalcone derivatives, we measured thermograms of **1**–**4** from room temperature to 400 °C in inert N_2 environment, as shown in Fig. 6. Prominent and sharp endothermic peaks, which represent their melting points, are evident for all the derivatives. Chalcones **1** and **4** show characteristic endothermic peaks at 154 and 93 °C, respectively, without any evidence of phase transition before these temperatures. In contrast, **2** and **3** show a number of phase-transition peaks before their melting temperatures, which present as sharp endothermic peaks at 205 and 167 °C, respectively. From the sharp peaks shown in Fig. 6, all derivatives are assumed to be highly crystalline and quite pure. The melting process continued up to the next exothermic peaks observed at 227, 234, and 230 °C for chalcones **1**, **2**, and **3**, respectively, and up to an endothermic peak at 178 °C for chalcone **4**. As the temperature increased above these values, the chalcone derivatives decomposed into highly viscous materials and eventually into gaseous end products [47,48]. In Fig. 6, decomposition near the melting point temperature is not evident, suggesting that these materials would be useful for laser applications, where high stability of the crystal at high temperature is required.

Conclusions

In summary, this work presented the preparation of four hydroxy-functionalized chalcones and their characterization using various spectroscopic techniques. The experimental vibrational and absorption spectra were successfully compared and interpreted with respect to the theoretical spectra obtained from DFT-optimized results at the B3LYP/6-31G(d,p) level. For the first time, we interpreted and correlated the IR and Raman spectra of four hydroxy-functionalized chalcones both experimentally and theoretically. It was determined that the synthesized chalcone derivatives are semiconducting materials because of their band-gaps, which were calculated from the absorption spectra, are between 0.5 and 4.0 eV. Their potential for application in the development of OLEDs was suggested from their dual and broad emission bands.

Acknowledgements

This work was financially supported by National Research Foundation of Korea (NRF) grants funded by the Korean government (MEST and MSIP) (2007-0056095, 2012K2A1A2033072, 2013S1A2A2035406, and 2013R1A1A2009575).

Appendix A. Supplementary data

Supplementary data associated with this article can be found, in the online version, at http://dx.doi.org/10.1016/j.saa.2015.05.085.

References

[1] J.C. Espinoza-Hicks, L.M. Rodriguez-Valdez, G.V. Nevarez-Moorillon, A. Camacho-Davila, J. Mol. Struct. 1020 (2012) 88–95.
[2] H.K. Hsieh, T.H. Lee, J.P. Wang, J.J. Wang, C.N. Lin, Pharm. Res. 15 (1998) 39–46.
[3] M. Cabrera, M. Simoens, G. Falchi, M.L. Lavaggi, O.E. Piro, E.E. Castellano, A. Vidal, A. Azqueta, A. Monge, A. López de Ceráin, G. Sagrera, G. Seoane, H. Cerecetto, M. González, Bioorg. Med. Chem. 15 (2007) 3356–3367.
[4] B.A. Bhat, K.L. Dhar, S.C. Puri, A.K. Saxena, M. Shanmugavel, G.N. Qazi, Bioorg. Med. Chem. 15 (2005) 3177–3180.
[5] C. Pouget, F. Lauthier, A. Simon, C. Fagnere, J.P. Basly, C. Delage, A.J. Chulia, Bioorg. Med. Chem. Lett. 11 (2001) 3095–3097.
[6] P.R. Bangal, S. Lahiri, S. Kar, S. Chakravorti, J. Lumin. 69 (1996) 49–56.
[7] F.A. Tarek, Chem. Phys. 324 (2006) 631–638.
[8] R. Rajalakshmi, D. Chinnaraja, J. Jayabharathi, Spectrochim. Acta Part A Mol. Biomol. Spectrosc. 117 (2014) 186–190.
[9] K. Rurack, J.L. Bricks, G. Reck, R. Radeglia, U. Resch-Genger, J. Phys. Chem. A 104 (2000) 3087–3109.
[10] B. Gu, W. Ji, P.S. Patil, S.M. Dharmaprakash, J. Appl. Phys. 103 (2008) 103511–103516.
[11] L. Mager, C. Melzer, M. Barzoukas, A. Fort, S. Mery, J.F. Nicoud, Appl. Phys. Lett. 71 (1997) 2248–2250.
[12] D. Millan, M. Dominguez, M.C. Rezende, Dyes Pigments 77 (2008) 441–445.
[13] T. Okuyama, M. Takata, J. Takayasu, T. Hasegawa, H. Tokuda, H. Nishino, A. Iwashima, Planta Med. 57 (1991) 242–246.
[14] R. Nishimura, K. Tabata, M. Arakawa, Y. Ito, Y. Kimura, T. Akihisa, H. Nagai, A. Sakuma, H. Kohno, T. Suzuki, Biol. Pharm. Bull. 30 (2007) 1878–1883.
[15] Y.L. Hsu, P.L. Kuo, W.S. Tzeng, C.C. Lin, Food Chem. Toxicol. 44 (2006) 704–713.
[16] T. Enoki, H. Ohnogi, K. Nagamine, Y. Kudo, K. Sugiyama, M. Tanabe, E. Kobayashi, H. Sagawa, I. Kato, J. Agric. Food Chem. 55 (2007) 6013–6017.
[17] S.K. Awasthi, N. Mishra, B. Kumar, M. Sharma, A. Bhattacharya, L.C. Mishra, V.K. Bhasin, Med. Chem. Res. 18 (2009) 407–420.
[18] P.M. Sivakumar, P.K. Prabhakar, M. Doble, Med. Chem. Res. 19 (2010) 1–17.
[19] K.L. Lahtchev, D.I. Batovska, S.P. Parushev, V.M. Ubiyvovk, A.A. Sibirny, Eur. J. Med. Chem. 43 (2008) 2220–2228.
[20] Y.S. Lee, S.S. Lim, K.H. Shin, Y.S. Kim, K. Ohuchi, S.H. Jung, Biol. Pharm. Bull. 29 (5) (2006) 1028–1031.
[21] F. Jin, X.Y. Jin, Y.L. Jin, D.W. Sohn, S.A. Kim, D.H. Sohn, Y.C. Kim, H.S. Kim, Arch. Pharm. Res. 30 (2007) 1359–1367.
[22] C.S. Chidan Kumar, H.K. Fun, C. Parlak, L. Rhyman, P. Ramasami, M. Tursun, S. Chandraju, C.K. Quah, Spectrochim. Acta Part A 132 (2014) 174–182.
[23] K. Baba, M. Taniguchi, K. Nakata, J. Jpn. 178 (1998) 52–60.
[24] K. Sugamoto, Y.I. Matsusita, K. Matsui, C. Kurogi, T. Matsui, Tetrahedron 67 (2011) 5346–5359.
[25] A. Zarghi, T. Zebardast, F. Hakimion, F.H. Shirazi, P.N.P. Rao, E.E. Knaus, Bioorg. Med. Chem. 14 (2006) 7044–7050.
[26] B. Srinivasan, T.E. Johnson, R. Lad, C. Xing, J. Med. Chem. 52 (2009) 7228–7235.
[27] N.B. Debattista, N.B. Pappano, Talanta 44 (1997) 1967–1971.
[28] H.Y. Wang, X.X. Zhang, J.J. Shi, G. Chen, X.P. Xu, S.J. Ji, Spectrochim. Acta Part A 93 (2012) 343–347.
[29] P. Hohenberg, W. Kohn, Phys. Rev. 136 (1964) B864.
[30] W. Kohn, L.J. Sham, Phys. Rev. 140 (1965) A1133.
[31] A.D. Becke, J. Chem. Phys. 98 (1993) 5648.
[32] C. Lee, W. Yang, R.G. Parr, Phys. Rev. B 37 (1988) 785.
[33] P.C. Hariharan, J.A. Pople, Theoret. Chim. Acta 28 (1973) 213.

[34] M.M. Francl, W.J. Pietro, W.J. Hehre, J.S. Binkley, M.S. Gordon, D.J. DeFrees, J.A. Pople, J. Chem. Phys. 77 (1982) 3654.
[35] B. Mennucci, E. Cancès, J. Tomasi, J. Phys. Chem. B 101 (1997) 10506.
[36] E. Cancès, B. Mennucci, J. Tomasi, J. Chem. Phys. 107 (1997) 3032.
[37] M.J. Frisch, G.W. Trucks, H.B. Schlegel, G.E. Scuseria, M.A. Robb, J.R. Cheeseman, G. Scalmani, V. Barone, B. Mennucci, G.A. Petersson, H. Nakatsuji, M. Caricato, X. Li, H.P. Hratchian, A.F. Izmaylov, J. Bloino, G. Zheng, J.L. Sonnenberg, M. Hada, M. Ehara, K. Toyota, R. Fukuda, J. Hasegawa, M. Ishida, T. Nakajima, Y. Honda, O. Kitao, H. Nakai, T. Vreven, J.A. Montgomery, Jr., J.E. Peralta, F. Ogliaro, M. Bearpark, J.J. Heyd, E. Brothers, K.N. Kudin, V.N. Staroverov, R. Kobayashi, J. Normand, K. Raghavachari, A. Rendell, J.C. Burant, S.S. Iyengar, J. Tomasi, M. Cossi, N. Rega, N.J. Millam, M. Klene, J.E. Knox, J.B. Cross, V. Bakken, C. Adamo, J. Jaramillo, R. Gomperts, R.E. Stratmann, O. Yazyev, A.J. Austin, Cammi, C. Pomelli, J.W. Ochterski, R.L. Martin, K. Morokuma, V.G. Zakrzewski, G.A. Voth, P. Salvador, J.J. Dannenberg, S. Dapprich, A.D. Daniels, O. Farkas, J.B. Foresman, J.V. Ortiz, J. Cioslowski, D.J. Fox, Gaussian Inc., Gaussian 09, Revision A.01, Wallingford CT, 2009.
[38] T. Teshima, M. Takeishi, T. Arai, New J. Chem. 33 (2009) 1393–1401.
[39] R.N. Singh, V. Baboo, P. Rawat, A. Kumar, D. Verma, Spectrochim. Acta Part A 94 (2012) 288–301.
[40] A. Nataraj, V. Balachandran, T. Karthick, J. Mol. Struct. 1031 (2013) 221–233.
[41] V. Balachandran, V. Karpagam, J. Mol. Struct. 1038 (2013) 52–61.
[42] M. Jagadeesh, H.K. Rashmi, Y. Subba Rao, A. Sreenath Reddy, B. Prathima, P. Uma Maheswari Devi, A. Varada Reddy, Spectrochim. Acta Part A 115 (2013) 583–587.
[43] H.G.O. Alvim, E.L. Fagg, A.L. de Oliveira, H.C.B. de Oliveira, S.M. Freitas, M.A.E. Xavier, T.A. Soares, A.F. Gomes, F.C. Gozzo, W.A. Silva, B.A.D. Neto, Org. Biomol. Chem. 11 (2013) 4764–4777.
[44] M. Maczka, W. Zierkiewicz, D. Michalska, J. Hanuza, Spectrochim. Acta Part A Mol. Biomol. Spectrosc. 128 (2014) 674–680.
[45] S. Ramachandran, G. Velraj, Rom. J. Phys. 58 (2013) 305–317.
[46] F.A. Tarek, M.K. Awad, Chem. Phys. 303 (2004) 317–326.
[47] P.S. Patil, S.M. Dharmaprakash, K. Ramakrishna, H.K. Fun, R.S.S. Kumar, D. Narayana Rao, J. Cryst. Growth 303 (2007) 520–524.
[48] V. Shettigar, P.S. Patil, S. Naveen, S.M. Dharmaprakash, M.A. Sridhar, J.S. Prasad, J. Cryst. Growth 295 (2006) 44–49.